JACS
JOURNAL OF THE AMERICAN CHEMICAL SOCIETY

Communication

pubs.acs.org/JACS

A $CsPbBr_3$ Perovskite Quantum Dot/Graphene Oxide Composite for Photocatalytic CO_2 Reduction

Yang-Fan Xu,[†] Mu-Zi Yang,[†] Bai-Xue Chen, Xu-Dong Wang, Hong-Yan Chen, Dai-Bin Kuang,* and Cheng-Yong Su

MOE Key Laboratory of Bioinorganic and Synthetic Chemistry, Lehn Institute of Functional Materials, School of Chemistry, Sun Yat-sen University, Guangzhou 510275, P. R. China

Supporting Information

ABSTRACT: Halide perovskite quantum dots (QDs), primarily regarded as optoelectronic materials for LED and photovoltaic devices, have not been applied for photochemical conversion (e.g., water splitting or CO_2 reduction) applications because of their insufficient stability in the presence of moisture or polar solvents. Herein, we report the use of $CsPbBr_3$ QDs as novel photocatalysts to convert CO_2 into solar fuels in nonaqueous media. Under AM 1.5G simulated illumination, the $CsPbBr_3$ QDs steadily generated and injected electrons into CO_2, catalyzing CO_2 reduction at a rate of 23.7 μmol/g h with a selectivity over 99.3%. Additionally, through the construction of a $CsPbBr_3$ QD/graphene oxide ($CsPbBr_3$ QD/GO) composite, the rate of electron consumption increased 25.5% because of improved electron extraction and transport. This study is anticipated to provide new opportunities to utilize halide perovskite QD materials in photocatalytic applications.

Due to the superfluous consumption of fossil fuels and unrestricted anthropogenic emissions of carbon dioxide (CO_2), a notorious greenhouse gas, levels of CO_2 are rapidly increasing in the atmosphere. Accordingly, besides photosynthesis and underground mineralization, which are conducted in nature, efficient alternative strategies for CO_2 valorization and fixation are significantly needed in current society.[1] Due to pioneering works in the 1970s, the innovation of artificial photosynthesis, which is driven by inexhaustible and clean solar energy, provides a valid route for the photochemical reduction of CO_2 to mitigate the environmental issues caused by CO_2 emissions.[2,3] Moreover, instead of the carbohydrates produced in natural photosynthesis, artificial solar-driven CO_2 reduction produces partially reduced compounds (carbon monoxide [CO], methane [CH_4], methanol [CH_3OH], etc.), which are common chemical fuels. Therefore, the development of photocatalytic CO_2 reduction technology is important to simultaneously resolve environmental issues and alleviate the energy crisis.

Thus, far, many semiconductors (e.g., TiO_2, CdS, C_3N_4, Cu_2O, and perovskite oxides) have been reported for the light-driven photoreduction of CO_2.[4−13] However, the search for a better candidate has not ceased. Recent and rapid developments in organic−inorganic halide perovskite materials have triggered great interest among researchers for their optoelectronic applications, especially in photovoltaic devices, because of the high extinction coefficients, wide absorption ranges, and long electron−hole diffusion lengths of these materials.[14−16] Remarkable photoelectric conversion efficiencies have been achieved for perovskite solar cells (PSCs) within just a few years of research (from 3.8% to 22.1%).[17] Inspired from the achievements in solar cells, halide perovskite materials are strong candidates for conducting efficient photosynthesis if the extreme characteristic instability issues of halide perovskite materials can be resolved first.[18,19] Recently, for the first time, K. T. Nam et al. reported that methylammonium lead iodide ($MAPbI_3$) powder could drive the photocatalytic splitting of HI for hydrogen (H_2) evolution and that $MAPbI_3$ was stable in a series of saturated aqueous solutions after precisely controlling the ion concentrations (H^+ and I^-).[20]

Herein, we focus on $CsPbBr_3$, a typical halide perovskite material with competing optoelectronic properties but preferable stability when compared to its organic−inorganic hybrid counterparts.[21] Both $CsPbBr_3$ quantum dots (QDs) and a $CsPbBr_3$ QD/graphene oxide ($CsPbBr_3$ QD/GO) composite were designed for the photocatalytic reduction of CO_2 to ethyl acetate (as depicted in Figure 1). To the best of our knowledge, this is the first report on artificial photosynthesis based on halide perovskite QDs.

A simple room-temperature antisolvent precipitation method was leveraged to synthesize the $CsPbBr_3$ QDs and $CsPbBr_3$ QD/GO composite material (details are provided in the Supporting Information).[22] Both as-prepared samples pos-

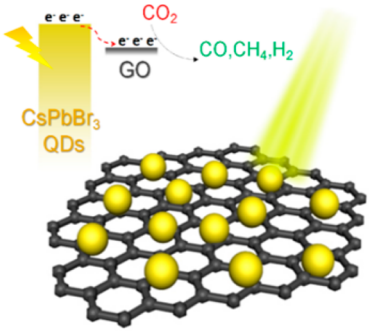

Figure 1. Schematic diagram of CO_2 photoreduction over the $CsPbBr_3$ QD/GO photocatalyst.

Received: January 16, 2017
Published: April 6, 2017

DOI: 10.1021/jacs.7b00489
J. Am. Chem. Soc. 2017, 139, 5660−5663

sessed visible-light absorption behavior and had strong photoinduced luminescence under UV-light stimulation, as depicted in Figure S1a and S1b. The powder X-ray diffraction (PXRD) patterns (Figure S1c) demonstrated that all the peaks of the as-prepared samples were indexed to the pure orthorhombic phase, and the broadened peaks indicated the reduction of the particle sizes. The transmission electron microscopy (TEM) image in Figure 2a shows the spherical

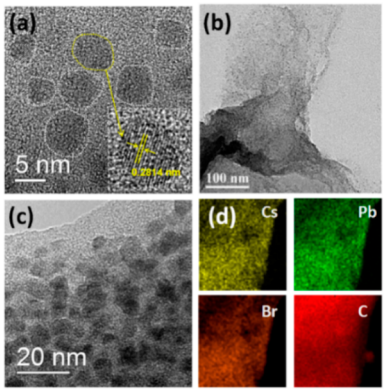

Figure 2. (a) HRTEM image of the $CsPbBr_3$ QDs; (b–d) TEM and HRTEM images of the $CsPbBr_3$ QD/GO and the corresponding EDX mapping images.

shape of the $CsPbBr_3$ QDs with sizes of approximately 6 ± 1 nm, according to the size distribution statistics in Figure S2. As shown in the inset of Figure 2a, a lattice spacing of 0.2814 nm, corresponding to the (220) plane, was clearly observed, which revealed that the $CsPbBr_3$ particles were highly crystalline. The TEM images of the as-prepared GO are shown in Figure S3, demonstrating a sheet-like morphology and characteristic graphitization at the edges. The Raman spectrum (Figure S4) of the as-prepared GO displayed two prominent peaks, the D band (1599 cm^{-1}) and G band (1360 cm^{-1}), with a peak height ratio (I_D/I_G) of 1.27. After introducing GO, the $CsPbBr_3$ QDs were evenly distributed on the GO sheets (Figure 2b). The size and crystallinity of the $CsPbBr_3$ QDs remained identical, as concluded from the high-resolution TEM (HRTEM) image in Figure 2c and the statistics in Figure S2b. Moreover, the energy-dispersive X-ray (EDX) mappings of Cs, Pb, Br, and C further confirmed the existence and uniform dispersion of the $CsPbBr_3$ QDs on GO. Furthermore, X-ray photoelectron spectroscopy (XPS) characterizations were performed to characterize the surface. The high-resolution plots of Cs 3d, Pb 4f, and Br 3d (Figure S5) demonstrated that their respective binding energies were in accordance with those presented in previous reports[23,24] and were unchanged after introducing GO. Notably, Br-rich surfaces were observed, as concluded from the surface atomic ratios summarized in Table S1, which may result in a self-passivation effect to alleviate the surface states.[23] To evaluate the mass ratio of QDs to GO, thermogravimetric analysis (TGA) was performed. The GO mass ratio in the composite was ~8.73% according to the TGA plots in Figure S6.

The as-prepared $CsPbBr_3$ QDs and $CsPbBr_3$ QD/GO composite were used as photocatalysts for artificial CO_2 reduction. QD photocatalysts have attracted widespread attention because of their high surface areas and short charge-transfer pathways.[25] Moreover, the enlarged bandgap and shifted band position caused by quantum-size confinement[26] can provide more potential energy to sufficiently drive photochemical reactions. In this study, the CO_2 reduction experiments were conducted in a sealed Pyrex bottle with ethyl acetate as the solvent. Ethyl acetate was selected because its mild polarity can stabilize the $CsPbBr_3$ QDs and because CO_2 is highly soluble in ethyl acetate (e.g., 241.0 mM, which is more than 7 times the solubility of CO_2 in water).[27] Light was provided by a 100-W Xe lamp with an AM 1.5G filter to simulate solar light illumination. Figure 3 and Table 1 present

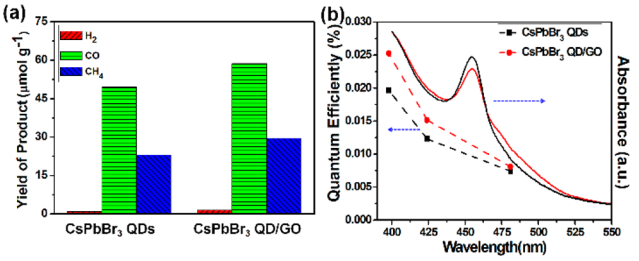

Figure 3. (a) Photocatalytic performance: yield of the CO_2 reduction products after 12 h of photochemical reaction. (b) UV–vis absorption spectra and the external quantum efficiency plots.

Table 1. Summary of the Photocatalytic CO_2 Reduction Performances after 12 h of Constant Illumination

Sample	R(CO)/ μmol g^{-1}	R(CH_4)/ μmol g^{-1}	R(H_2)/ μmol g^{-1}	$R_{electron}$ [a]/ μmol g^{-1}	select. for CO_2 red.[b]/%
$CsPbBr_3$ QDs	49.5	22.9	1.07	284.7	99.3
$CsPbBr_3$ QD/GO	58.7	29.6	1.58	357.4	99.1

[a] $R_{electron}$ is the rate of electron consumption for the reduced product; $R_{electron} = 2R(CO) + 8R(CH_4) + 2R(H_2)$. [b] Selectivity for CO_2 reduction = $[2R(CO) + 8R(CH_4)]/R_{electron} \times 100\%$.

the amounts of CH_4 and H_2 produced after 12 h of photocatalytic CO_2 reduction. The concentrations of all the products increased linearly with time (Figure S7), the averaged electron consumption ($R_{electron}$) for the $CsPbBr_3$ QDs was 23.7 μmol/g h throughout the reaction, and an $R_{electron}$ of 29.8 μmol/g h was observed for the $CsPbBr_3$ QD/GO composite. These rates are superior to those of CdS and other newly developed photocatalysts with visible-light responses under Xe-lamp illumination (Table S1). Notably, the selectivity for CO_2 reduction was impressively greater than 99%, implying the efficient suppression of the H_2 evolution reaction in the nonaqueous solvent. However, part of the CO yield potentially originates from the partial photooxidation of ethyl acetate, which was evidenced via a control experiment using an inert N_2 instead of a saturated CO_2 atmosphere. Under the same illumination conditions, CO and CO_2 were generated with an average rate of 0.56 and 2.52 μmol/g h by the $CsPbBr_3$ QDs, respectively. In other words, the CO yield under N_2 was one-eighth that under saturated CO_2, and most of the solar fuels originated from photocatalytic CO_2 reduction by the photocatalysts. Since the stability of the photocatalyst is another critical issue for practical applications, the PXRD patterns of both the individual $CsPbBr_3$ QDs and the $CsPbBr_3$ QD/GO composite after 12 h of photocatalytic reaction were recorded. As shown in Figure S8, neither phase transformation nor degradation to impurities (e.g., $CsPb_2Br_5$) were observed. XPS results further elucidated that both the chemical states and the surface elemental compositions remained unchanged when

DOI: 10.1021/jacs.7b00489
J. Am. Chem. Soc. 2017, 139, 5660–5663

comparing the as-prepared photocatalyst with the spent photocatalyst (Table S1, Figure S5).

External quantum efficiency (EQE) tests were also conducted as a function of wavelength. As illustrated in Figure 3b, the $CsPbBr_3$ QD/GO composite achieved a better EQE than the individual $CsPbBr_3$ QDs in the entire EQE test range. The EQE is composed of the light harvesting efficiency (LHE) and the charge-separation and charge-injection efficiencies.[28] However, the similar absorption behavior of the individual $CsPbBr_3$ QDs and the $CsPbBr_3$ QD/GO composite recorded in UV–vis absorption spectra (Figure 3b) indicated that the charge-transport and charge-injection efficiencies rather than the similar LHE were potentially responsible for the difference of the EQE.

To clarify the role of GO on enhancing the CO_2 reduction rate, further photoluminescence (PL) and electrochemical characterizations were conducted. First, the PL intensity and lifetime were probed to investigate the electron-transfer properties. As shown in Figure 4a, the steady-state PL spectra

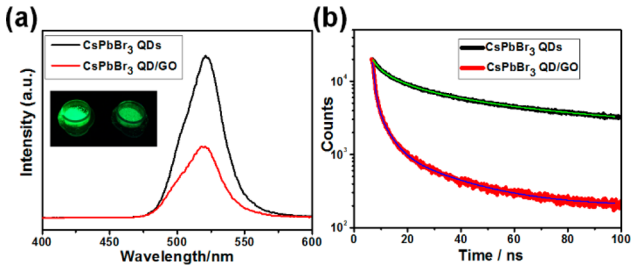

Figure 4. (a) Steady-state PL spectra with an excitation wavelength of 369.6 nm. (b) PL decay spectra after pulsed excitation at λ = 369.6 nm.

illustrated that the PL intensity of the $CsPbBr_3$ QD/GO composite decreased to a lower level than that of the pristine $CsPbBr_3$ QDs because the introduction of graphene provided an additional energy-transfer pathway in addition to the intrinsic radiative channel for excited-state electron transfer. In the $CsPbBr_3$ QD/GO composite, excited electrons in the $CsPbBr_3$ QDs will rapidly transfer to the GO since the Fermi level of GO is more positive than the conduction band edge of $CsPbBr_3$ and due to the conductive nature of GO.[9,29,30] Therefore, quick separation of photogenerated electron–hole pairs and suppressed charge recombination will occur, which finally results in quenching of the PL intensity.[31−33] This conclusion was also confirmed by the band alignment of the $CsPbBr_3$ QDs, which was detected by XPS (Figure S9) and indicates the existence of graphene was in favor of the facile charge transfer. Quenching of the PL intensity was also observed from photographs of the $CsPbBr_3$ QDs and the $CsPbBr_3$ QD/GO composite powders under UV-light stimulation (Figure 4a, inset). Furthermore, the normalized time-resolved PL decay plots after pulsed laser excitation at λ = 369.6 nm (Figure 4b) confirmed the fast charge separation by graphene. The decay traces were fitted using triexponential decay kinetics with low uncertainties (χ), and the parameters are listed in Table 2. Both the $CsPbBr_3$ QDs and the $CsPbBr_3$ QD/GO composite exhibited a PL decay time on the nanosecond scale, which are consistent with previous reports.[22,34] The $CsPbBr_3$ QD/GO composite decayed distinctly faster than the pristine $CsPbBr_3$ QDs, with average PL decay times ($\tau_{average}$) of 11.3 and 38.3 ns for the $CsPbBr_3$ QD/GO composite and the $CsPbBr_3$ QDs, respectively.

Table 2. PL Decay Parameters of the $CsPbBr_3$ QDs and $CsPbBr_3$ QD/GO

	τ_1	τ_2	τ_3	$\tau_{average}$	χ
$CsPbBr_3$ QDs	2.25	8.84	44.7	38.3	1.09
$CsPbBr_3$ QD/GO	0.839	4.08	22.4	11.3	1.25

Additionally, the contributions of the components with fast decay times (τ_1 and τ_2, which are related to charge transfer)[35,36] increased from 17.5% to 57.7%, illustrating the considerable interaction between the $CsPbBr_3$ QDs and GO.[32] The decrease of the PL intensity by nearly one-half and the accelerated PL decay confirmed that rapid charge transfer occurred between the $CsPbBr_3$ QDs and GO, hence partially addressing the proverbial severe surface charge recombination issues in individual QD photocatalysts.[37]

Furthermore, the photoelectrochemical (PEC) performances were investigated by constructing a PEC cell. First, the photoelectrodes were assembled. As shown in Figure S10a–b, the two centrifugally casted thin films had thicknesses of 500 nm and were compact. The PL behavior under UV-light stimulation was well preserved (Figure S10c–d). The amperometric I–t curves (Figure 5a) plotted at −0.4 $V_{Ag/AgCl}$

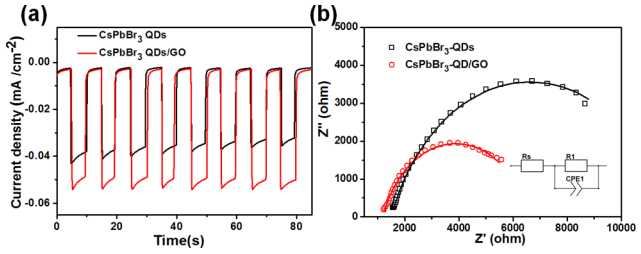

Figure 5. (a) Amperometric I–t curves plotted at −0.4 $V_{Ag/AgCl}$ under chopped AM 1.5G illumination. (b) EIS Nyquist plots recorded under 150 mW cm^{-2} illumination at a bias of −0.4 $V_{Ag/AgCl}$; the lines are the corresponding fitted results. Inset is the equivalent circuit model.

demonstrated that the photocurrent was highly repeatable upon cycling the light on and off. The photocurrent response of the $CsPbBr_3$ QD/GO sample was 54 μA cm^{-2}, corresponding to a 28.57% enhancement compared to the $CsPbBr_3$ QDs (42 μA cm^{-2}), which agrees with the $R_{electron}$ in the photocatalytic characterizations. Electrochemical impedance spectroscopy (EIS) was further employed to detect the charge-transport behaviors of these two electrodes. As shown in Figure 5b, the Nyquist plots indicated that the charge-transfer resistance obviously decreased for the $CsPbBr_3$ QD/GO film, as evidenced by the smaller semicircle arc at high frequencies and the corresponding fitting results (10 238 ohms for $CsPbBr_3$ QDs and 5387 ohms for $CsPbBr_3$ QD/GO). The pronounced decrease of the charge-transfer resistance by incorporating GO clearly validates the better charge transport ability of the GO composite.

In summary, we demonstrated the utilization of a $CsPbBr_3$ QD/GO material for the photochemical conversion of CO_2 for the first time. Compared to the individual $CsPbBr_3$ QDs, the rate of electron consumption improved from 23.7 to 29.8 μmol/g h after the introduction of GO. The PL and photoelectrochemical impedance tests confirmed that the photocatalytic enhancement was caused by the electron-extraction ability of conductive GO. As a proof of concept, our study paves the way for using halide perovskite materials

DOI: 10.1021/jacs.7b00489
J. Am. Chem. Soc. 2017, 139, 5660−5663

and their composites for highly efficient and stable photocatalytic or photoelectrochemical reduction of CO_2.

■ ASSOCIATED CONTENT

Supporting Information

The Supporting Information is available free of charge on the ACS Publications website at DOI: 10.1021/jacs.7b00489.

Experimental details (PDF)

■ AUTHOR INFORMATION

Corresponding Author

*kuangdb@mail.sysu.edu.cn

ORCID

Yang-Fan Xu: 0000-0002-4479-6157

Dai-Bin Kuang: 0000-0001-6773-2319

Cheng-Yong Su: 0000-0003-3604-7858

Author Contributions

†Y.-F.X. and M.-Z.Y. contributed equally

Notes

The authors declare no competing financial interest.

■ ACKNOWLEDGMENTS

The authors acknowledge financial support from the National Natural Science Foundation of China (91433109, 91222201), GDUPS (2016), the Program of Guangzhou Science and Technology (201504010031), the Fundamental Research Funds for the Central Universities, and the NSF of Guangdong Province (S2013030013474, 2014A030313148).

■ REFERENCES

(1) Maginn, E. J. *J. Phys. Chem. Lett.* **2010**, *1*, 3478−3479.
(2) Halmann, M. *Nature* **1978**, *275*, 115−116.
(3) Fujishima, A.; Honda, K. *Nature* **1972**, *238*, 37−38.
(4) Neatu, S.; Maciá-Agullò, J. A.; Concepciòn, P.; Garcia, H. *J. Am. Chem. Soc.* **2014**, *136*, 15969−15976.
(5) Wang, S. B.; Wang, X. C. *Appl. Catal., B* **2015**, *162*, 494−500.
(6) Fujiwara, H.; Hosokawa, H.; Murakoshi, K.; Wada, Y.; Yanagida, S.; Okada, T.; Kobayashi, H. *J. Phys. Chem. B* **1997**, *101*, 8270−8278.
(7) Zheng, Y.; Lin, L. H.; Ye, X. J.; Guo, F. S.; Wang, X. C. *Angew. Chem., Int. Ed.* **2014**, *53*, 11926−11930.
(8) Gao, G.; Jiao, Y.; Waclawik, E. R.; Du, A. *J. Am. Chem. Soc.* **2016**, *138*, 6292−6297.
(9) Hou, J. G.; Cheng, H. J.; Takeda, O.; Zhu, H. *Angew. Chem., Int. Ed.* **2015**, *54*, 8480−8484.
(10) Schreier, M.; Luo, J. S.; Gao, P.; Moehl, T.; Mayer, M. T.; Grätzel, M. *J. Am. Chem. Soc.* **2016**, *138*, 1938−1946.
(11) Do, J. Y.; Im, Y.; Kwak, B. S.; Park, S.-M.; Kang, M. *Ceram. Int.* **2016**, *42*, 5942−5951.
(12) Kwak, B. S.; Kang, M. *Appl. Surf. Sci.* **2015**, *337*, 138−144.
(13) Wang, J.; Huang, C.; Chen, X.; Zhang, H.; Li, Z.; Zou, Z. *Appl. Surf. Sci.* **2015**, *358*, 463−467.
(14) Kazim, S.; Nazeeruddin, M. K.; Grätzel, M.; Ahmad, S. *Angew. Chem., Int. Ed.* **2014**, *53*, 2812−2824.
(15) He, M.; Zheng, D.; Wang, M.; Lin, C.; Lin, Z. *J. Mater. Chem. A* **2014**, *2*, 5994−6003.
(16) He, M.; Pang, X.; Liu, X.; Jiang, B.; He, Y.; Snaith, H.; Lin, Z. *Angew. Chem., Int. Ed.* **2016**, *55*, 4280−4284.
(17) http://www.nrel.gov/ncpv/images/efficiency_chart.jpg.
(18) Kim, Y.; Yassitepe, E.; Voznyy, O.; Comin, R.; Walters, G.; Gong, X.; Kanjanaboos, P.; Nogueira, A. F.; Sargent, E. H. *ACS Appl. Mater. Interfaces* **2015**, *7*, 25007−25013.
(19) Schmidt, L. C.; Pertegás, A.; González-Carrero, S.; Malinkiewicz, O.; Agouram, S.; Mínguez Espallargas, G.; Bolink, H. J.; Galian, R. E.; Pérez-Prieto, J. *J. Am. Chem. Soc.* **2014**, *136*, 850−853.
(20) Park, S.; Chang, W. J.; Lee, C. W.; Park, S.; Ahn, H.-Y.; Nam, K. T. *Nat. Energy* **2016**, *2*, 16185.
(21) Kulbak, M.; Gupta, S.; Kedem, N.; Levine, I.; Bendikov, T.; Hodes, G.; Cahen, D. *J. Phys. Chem. Lett.* **2016**, *7*, 167−172.
(22) Sun, S. B.; Yuan, D.; Xu, Y.; Wang, A. F.; Deng, Z. T. *ACS Nano* **2016**, *10*, 3648−3657.
(23) Li, X.; Wu, Y.; Zhang, S.; Cai, B.; Gu, Y.; Song, J.; Zeng, H. *Adv. Funct. Mater.* **2016**, *26*, 2435−2445.
(24) Zhang, F.; Zhong, H.; Chen, C.; Wu, X.-g.; Hu, X.; Huang, H.; Han, J.; Zou, B.; Dong, Y. *ACS Nano* **2015**, *9*, 4533−4542.
(25) Gellman, A. J.; Shukla, N. *Nat. Mater.* **2009**, *8*, 87−88.
(26) Smith, A. M.; Nie, S. *Acc. Chem. Res.* **2010**, *43*, 190−200.
(27) Hansen, C. M. *Hansen solubility parameters: A User's Handbook*, 2nd ed.; CRC Press: Boca Raton, FL, 2007.
(28) Dotan, H.; Sivula, K.; Grätzel, M.; Rothschild, A.; Warren, S. C. *Energy Environ. Sci.* **2011**, *4*, 958−964.
(29) Li, Q.; Li, X.; Wageh, S.; Al-Ghamdi, A. A.; Yu, J. *Adv. Energy Mater.* **2015**, *5*, 1500010.
(30) Huang, X.; Qi, X.; Boey, F.; Zhang, H. *Chem. Soc. Rev.* **2012**, *41*, 666−686.
(31) Yang, H. B.; Miao, J. W.; Hung, S. F.; Huo, F. W.; Chen, H. M.; Liu, B. *ACS Nano* **2014**, *8*, 10403−10413.
(32) Lightcap, I. V.; Kamat, P. V. *J. Am. Chem. Soc.* **2012**, *134*, 7109−7116.
(33) Kaniyankandy, S.; Rawalekar, S.; Ghosh, H. N. *J. Phys. Chem. C* **2012**, *116*, 16271−16275.
(34) Swarnkar, A.; Chulliyil, R.; Ravi, V. K.; Irfanullah, M.; Chowdhury, A.; Nag, A. *Angew. Chem., Int. Ed.* **2015**, *54*, 15424−15428.
(35) Zhang, Y. X.; Wang, H. Y.; Zhang, Z. Y.; Zhang, Y.; Sun, C.; Yue, Y. Y.; Wang, L.; Chen, Q. D.; Sun, H. B. *Phys. Chem. Chem. Phys.* **2017**, *19*, 1920−1926.
(36) Wu, K.; Liang, G.; Shang, Q.; Ren, Y.; Kong, D.; Lian, T. *J. Am. Chem. Soc.* **2015**, *137*, 12792−12795.
(37) Regulacio, M. D.; Han, M. Y. *Acc. Chem. Res.* **2016**, *49*, 511−519.

DOI: 10.1021/jacs.7b00489
J. Am. Chem. Soc. 2017, 139, 5660−5663